Aerodynamic Noise Reduction Using a Fine Grid Structure

M. Azarpeyvand

Institute of Sound and Vibration Research

University of Southampton

Southampton, SO17 1BJ, UK

Abstract

In this paper, we study the possibility of reduction of noise produced by turbulent flows using a fine grid structure. Although the concept has been widely used in turbulent flow studies for the purpose of creating homogeneous isotropic turbulent medium, it has never been systematically checked for aerodynamic noise reduction purposes. In this paper we shall confine ourselves to noise reduction of an unheated single-stream high Mach number jet. We shall make use of a RANS $k-\varepsilon$ turbulence model along with Lighthill's Acoustic Analogy in order to comprehensively examine this concept. Two different grid geometries located at three positions ($6D_J$, $8.6D_J$, and $12D_J$ from the jet exit) in a jet shear flow are considered. Results have shown that significant low frequency noise reduction can be achieved when the grid is positioned at the end of the jet potential core.

1 Introduction

Aerodynamic noise reduction requires prior knowledge of turbulence suppression. However, due to the chaotic nature of the turbulent flows this is far from an easy task. The turbulence reduction strategies generally fall into two main categories: active and passive. A list of these strategies and their reviews can be found in Refs. [1, 2]. It is normally believed that the turbulence is formed by some coherent structures and random motions. It is also found that up to 0.25 of the total turbulent energy content of the medium is associated with the coherent structures. Furthermore, it has been shown that the coherent structures are most amenable to external flow control [1]. On the other hand, from Lighthill's Acoustic Analogy studies, one can deduce that the noise source term strength is proportional to the seventh power of the turbulent kinetic energy value at the source position. An instant conclusion of the above deductions is that the noise reduction can be achieved by diminishing the coherent structures in the turbulent medium. However, the success of such a supposition heavily depends on the efficiency of the system utilized for filtering the coherent structures.

In this paper we only consider the passive control methods. Among all of the possible passive strategies used so far, special attention has been given to the use of grids. They have been used for many years to produce or suppress turbulence in wind tunnels and as the name of the strategy implies, it consists of a manipulator placed in the turbulent flow. Various manipulator structures have been utilized until now, such as honeycombs, bi-planar grids, Wicker grids, etc [3]. It is worth mentioning here that grids oscillating around a mean position have also been widely used and it is shown that they can produce faster turbulence decay than the fixed grids.

In incompressible flows, homogeneous isotropic turbulence (no production) has usually been experimentally approximated by grid-generated turbulence, the decay of which in the downstream of the

grid (x) is well-represented by the power law

$$\frac{k}{U^2} = A\left(\frac{x - x_0}{m}\right)^{-N} \tag{1}$$

where x_0 is the effective origin, and m is the element of spacing of the grid. The decay exponent N varies between 1.15 and 1.45, and the value of A varies widely depending on the geometry of the grid and the Reynolds number [4]. The decay exponent increases to about 2 for oscillating grids (*i.e.* active grids) [5, 6], which indicates a more rapid turbulence decay. It is important to note that the above relation holds only for incompressible flows. The turbulence decay for a compressible flow was considered in Ref. [7] and it was shown that the decay exponent is a parabolic function of Mach number (M), starting from $N = 1.27$ for $M = 0.16$ (incompressible range), reaching its minimum $N = 0.85$ at about $M = 0.3$, and then increasing with Mach number.

In spite of numerous applications of grids and screens in wind tunnels and turbulence studies during the past century, the idea has never been used in aero-acoustics. As mentioned above, by using a grid, one can break the large powerful eddies (*i.e.* low frequency noise source) into some smaller and weaker eddies. In other words, by locating a grid near the most energetic noise sources, we must be able to lessen their power, and therefor the radiated noise from that region. In this study, we shall present a systematic way to tackle an aeroacoustic problem. Here, with no loss of generality, we confine our attention to a round jet operating at $M = 0.75$, $T = 300K$. Although this particular example might not be industrially applicable for aircraft noise, but it still can be used for outdoor jet engine tests, which cause neighbors' discomfort and are usually the subject of their complaints.

In this paper, for the purpose of simplicity, we have only used arrays of circular bars, see figure 1. The bars are of rectangular and circular cross-sections. Although it is not difficult to extend this study to 3D, we only consider 2D cases here whose CFD simulations can be carried out much faster. The mean flow and turbulent parameters are found using a modified $k - \varepsilon$ RANS turbulence model. The

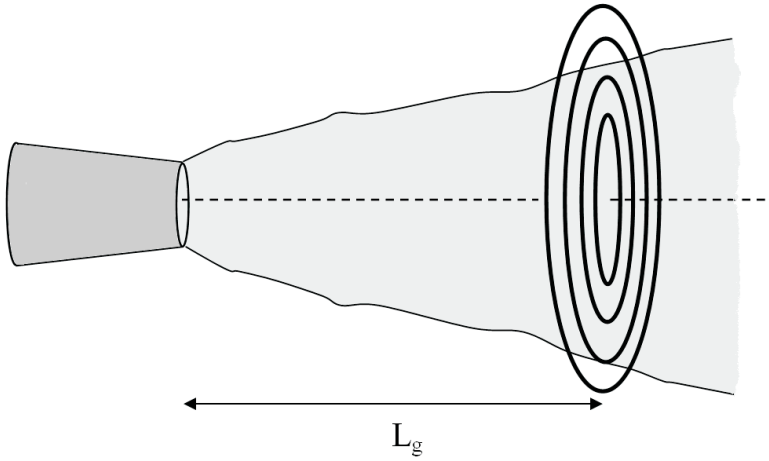

FIGURE 1: Problem geometry

CFD simulations have been performed for three grid locations, $6D_J$, $8.6D_J$, and $10D_J$. The CFD outcomes have then been used in Lighthill's Acoustic Analogy for finding the noise source strength and calculating the emanated noise to a far-field observer located at 90 degrees from the jet downstream axis.

The layout of the paper is as follows. In section 2 we shall provide the derivation of Lighthill's Acoustic Analogy, and explain how it is connected to the CFD results. The CFD simulations and discussions are then presented in Section 3. In Section 4 is presented the results and discussions for noise comparisons between an isolated jet and jet-grid simulations at three grid locations. Finally, Section 5 concludes the paper.

2 Acoustic Analogy

Lighthill's solution to the jet noise problem, usually referred to as Lighthill's Acoustic Analogy (AA), is actually a rearrangement of the equations of continuity and momentum to give the homogenous acoustic wave operator on the left hand side, and the terms remaining are placed on the right hand side and are viewed as the source terms. In this way the jet is viewed as a volume distribution of

quadruple sources that radiate sound into an ambient medium at rest. Lighthill's equation for density fluctuations is [8]

$$\frac{\partial^2 \rho'}{\partial t^2} - c_0^2 \nabla^2 \rho' = \frac{\partial^2 T_{ij}}{\partial x_i \partial x_j}, \tag{2}$$

where T_{ij} is the Lighthill stress tensor which (ignoring viscous terms) is given by:

$$T_{ij} = \rho u_i u_j + \delta_{ij} \left[(p - p_0) - c_0^2 (\rho - \rho_0) \right]. \tag{3}$$

For isothermal jets considered in this paper the second term is identically zero, and by decomposing the velocity in the usual way into mean and turbulent components as $u_i = U_i + v_i$ we follow a common assumption that an adequate approximation to the Lighthill tensor is given by

$$T_{ij} = \rho u_i u_j. \tag{4}$$

The density fluctuation for a far-field observer located at a distance x then be obtained using the free-space Green's function solution, [8]

$$\rho'(\mathbf{x}, t) = \frac{1}{4\pi x c^2} \int\limits_{V(\mathbf{y})} \frac{\partial^2}{\partial t^2} T_{(x,x)} \left\langle \mathbf{y}, t - |\mathbf{x} - \mathbf{y}| / c \right\rangle d\mathbf{y}. \tag{5}$$

The far field spectral intensity density, $S(x, \omega)$ can be found through the Fourier transform of the autocorrelation function of the far-field pressure $p' = c_0^2 \rho'$, [8]

$$S(x, t) = \frac{1}{32\pi^3 \rho c^2 x^2} \int\limits_{-\infty}^{\infty} \int\limits_{V(\mathbf{y}_1)} \int\limits_{V(\mathbf{y}_2)} \frac{\partial^4}{\partial \tau^4} \overline{T_{(x,x)} \left\langle \mathbf{y}_1, t \right\rangle T_{(x,x)} \left\langle \mathbf{y}_2, t + \tau + \tau^* \right\rangle} \, e^{j\omega\tau} d\mathbf{y}_1 d\mathbf{y}_2 d\tau, \tag{6}$$

where $\tau^* = |\mathbf{x}/x| \left[(\mathbf{y}_2 - \mathbf{y}_1)/c \right]$. The above equation contains a two-point correlation function which is measured in a fixed frame of reference. In order to take account of effects of source convection, one needs to convert this correlation function to a moving frame of reference. This can be carried out by

defining

$$\boldsymbol{\xi} = (\mathbf{y}_2 - \mathbf{y}_1) - \boldsymbol{i} c M_c \tau, \tag{7}$$

where $\boldsymbol{i}$ denotes the unit vector along the source-observer connecting line, and M_c is the local Mach number . Then, the spectral intensity density may be calculated from

$$S(x,t) = \frac{\rho\omega^4}{32\pi^3 c^2 x^2} \int_{-\infty}^{\infty} \int_{V(\mathbf{y}_1)} \int_{V(\mathbf{y}_2)} R^{(m)} \langle \mathbf{y}_1, \boldsymbol{\xi}, t \rangle \; e^{j\omega[(1-M_c\cos\theta)\tau - \frac{\mathbf{x}}{x}\cdot\frac{\boldsymbol{\xi}}{c}]} d\boldsymbol{\xi} d\mathbf{y}_1 d\tau, \tag{8}$$

where θ is the polar angle of the observer to the jet downstream axis direction, and $R^{(m)}$ is the two-point correlation function of the Lighthill stress tensor in the moving frame ξ, and is given by

$$R^{(m)} \langle \mathbf{y}_1, \boldsymbol{\xi}, t \rangle = \frac{\overline{T_{(x,x)} \langle \mathbf{y}_1, t \rangle \, T_{(x,x)} \langle \mathbf{y}_1 + \boldsymbol{\xi}, t \rangle}}{\rho^2 c^4}. \tag{9}$$

The correlation in the moving frame of reference can be modeled in various forms [9]. In this paper a Gaussian form is used

$$R^{(m)} \langle \mathbf{y}_1, \boldsymbol{\xi}, t \rangle = \Upsilon^2 \rho^2 k^4 e^{-\left(\frac{\xi}{l_0}\right)^2} e^{-\left(\frac{\tau}{\tau_0}\right)^2}, \tag{10}$$

where Υ is the source term amplitude factor, k being the turbulent kinetic energy (TKE) at the source location, and τ_0 and l_0 are the correlation time- and length-scales which are defined as [10]

$$l_0 = c_l \frac{k^{3/2}}{\varepsilon}, \tag{11}$$

$$\tau_0 = c_\tau \frac{k}{\varepsilon} \left(\frac{\Lambda}{l_0^*} \right). \tag{12}$$

The eddy size, Λ, can be estimated using either the shear layer thickness [11], or a frequency dependent length scale model [12, 13] (these two are however equivalent). In this comparison the latter model is

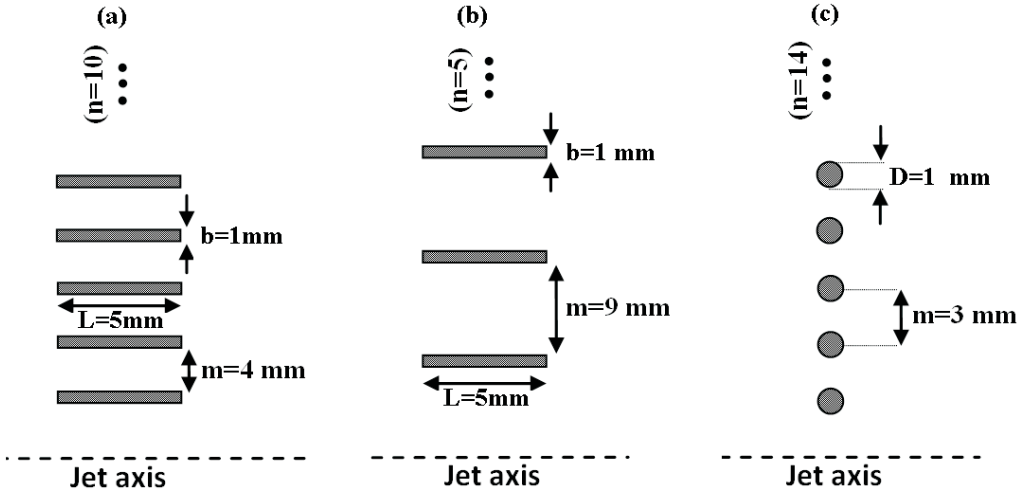

FIGURE 2: A schematic of the cross-section of the grids; (a) rectangular cross-section; $n = 10$, (b) rectangular cross-section; $n = 5$, (c) circular cross-section; $n = 14$.

used, as

$$\Lambda(\omega) = c_l D_J \frac{1 - e^{-c_s St.L/D_J}}{St}, \tag{13}$$

where l_0^* is the turbulence length scale, equation (11) (with $c_l = 1$), D_J is the jet nozzle diameter, c_s is a factor which determines the transition between the low and high frequency behaviors of the spectrum [13], and Strouhal number is defined as $St = fD_J/U_J$. The turbulent kinetic energy (k), the TKE dissipation rate (ε), and the local Mach number must be found from the CFD simulations.

3 CFD and Turbulence Modeling

A Reynolds Averaged Navier Stokes (RANS) scheme using a simple modified $k - \varepsilon$ turbulence model was used to achieve the required input for the acoustic source model. The following equations are solved using FUELNT software *V*.6.3.26:

$$\frac{\partial k}{\partial t} + U_j \frac{\partial k}{\partial x_j} = -\overline{v_i v_j} \frac{\partial U_i}{\partial x_j} - \varepsilon + \frac{\partial}{\partial x_j} \left[\left(\nu + \frac{\nu_T}{\sigma_k} \right) \frac{\partial k}{\partial x_j} \right], \tag{14}$$

$$\frac{\partial \varepsilon}{\partial t} + U_j \frac{\partial \varepsilon}{\partial x_j} = -C_{1\varepsilon} \frac{\varepsilon}{k} \overline{v_i v_j} \frac{\partial U_i}{\partial x_j} - C_{2\varepsilon} \frac{\varepsilon^2}{k} + \frac{\partial}{\partial x_j} \left[\left(\nu + \frac{\nu_T}{\sigma_\varepsilon} \right) \frac{\partial \varepsilon}{\partial x_j} \right], \tag{15}$$

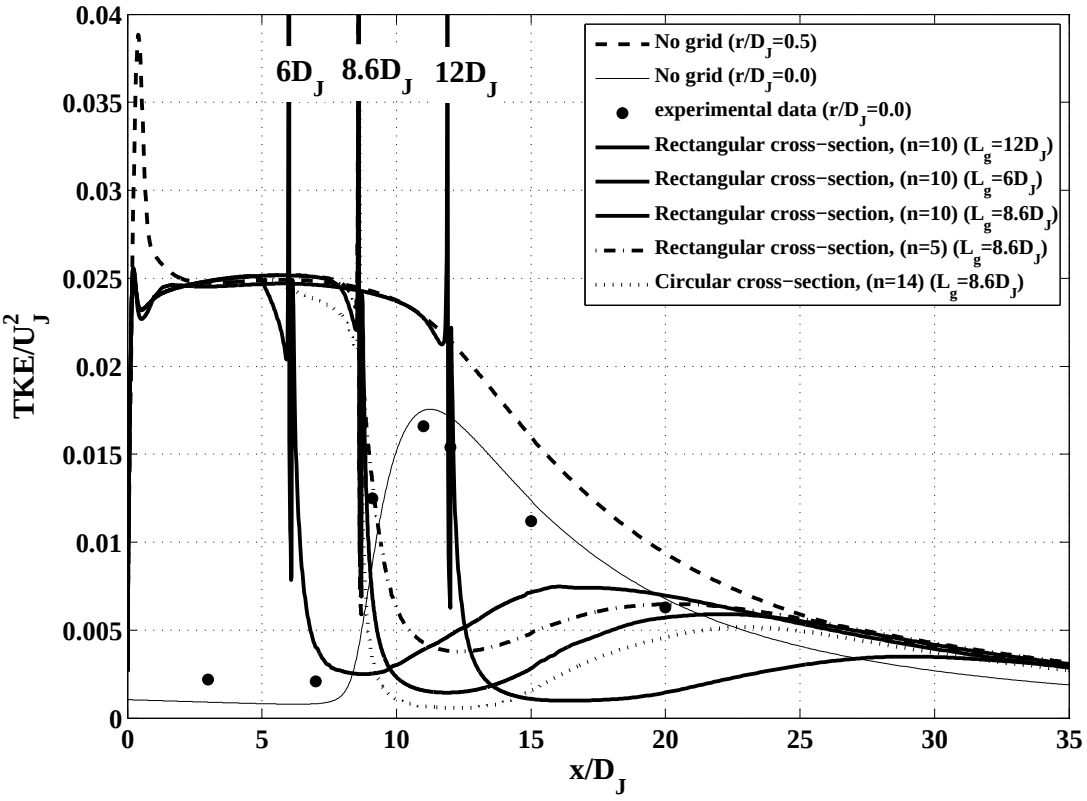

FIGURE 3: Normalized turbulent kinetic energy.

$$C_{1\varepsilon} = 1.44,\ C_{2\varepsilon} = 1.83,\ C_{\mu} = 0.09,\ \sigma_k = 1.0,\ \sigma_{\varepsilon} = 1.3, \tag{16}$$

$$l = C_{\mu} k^{3/2} \Big/ \varepsilon, \tag{17}$$

where equations (16) and (17) are the closure coefficients and auxiliary relations respectively, and $\nu_T = C_{\mu} k^2/\varepsilon$. The above system of equations are usually referred to as the RANS $k-\varepsilon$ model. In this paper, the value of $C_{2\varepsilon}$ is changed from the default value of 1.92 to 1.83 to reduce the spreading rate from 0.12 to 0.10 and get a better self-similarity agreement in the fully developed range [14]. The nozzle diameter is $49.75mm$, and the geometrical parameters of the grids can be seen in Figure 2.

In this part is presented the CFD results for different cases. As the figure shows the rods are distributed radially inside the turbulent flow, starting from the jet axis. Figure 3 illustrates the turbulent kinetic energy variation along the nozzle lip-line ($r/D_J = 0.5$) for six cases: The first case considers an isolated jet (no grid) at Mach number $M = 0.75$ at ambient temperature $T = 300K$. The TKE

variation along the jet axis ($r = 0$) is also presented and compared against the experimental data and shows a good level of agreement. The next three curves show the variation of TKE along the nozzle lip-line when a grid with rectangular cross-section is positioned at $6D_J$, $8.6D_J$ and finally $12D_J$ downstream. In these cases, the grid consists of a total number of 10 rods ($n = 10$). As expected, a sharp roll-off is observed beyond the grid location. This implies that the large coherent structures are now broken into some smaller eddies with maximum diameter of the grid spacing size. By decreasing the number of the rods to 5, the roll-off gets somewhat slower, but still an acceptable reduction in the TKE has been achieved. The last simulation is performed for a round grid with circular cross-section ($n = 14$). Comparisons show that the roll-off after the grid location is not very sensitive to the choice of the cross-section shape, but rather the grid spacing size. It can also be seen from the figure that the curves peak once more further downstream, about $10D_J$ to $15D_J$ after the grid, which is due to the fact that the production of TKE is not entirely vanished.

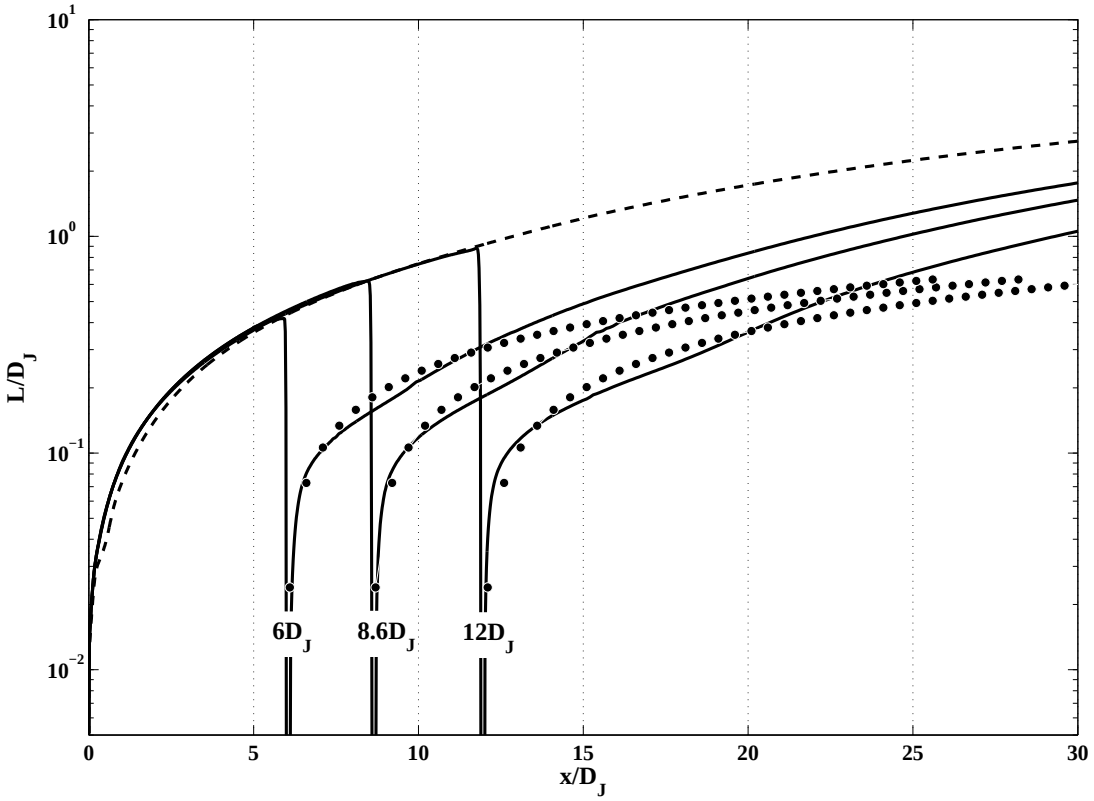

FIGURE 4: Normalized integral length-scale along the nozzle lip-line ($r = D_J/2$) for the rectangular cross-section grid ($n = 10$); Markers: Experimental curve-fit from Ref. [3]

Figure 4 presents the variation of the integral length-scale, equation (11) (with $c_l = 1$), along the nozzle lip-line for the rectangular cross-section grid ($n = 10$) at three positions ($6D_J$, $8.6D_J$, and $12D_J$). It can be seen that the large eddies are broken into some much smaller eddies (and much weaker) beyond the screening structure position. The behavior of the integral length-scale in a grid turbulence has been comprehensively studied in Ref. [3] and the curve-fits are provided for different types of grids. It was found that the experimental data can be fit by a straight line in log coordinates, as $\log L/L_* = p \log x/L_* + B$, where L_* is a grid length-scale parameter (usually rods spacing size, m), p is found to be usually around 0.62 for biplanar grids, and B varies widely from case to case. In figure 4 the black marker results are calculated using this curve-fit. Despite the agreement between the CFD results and the model in the first five diameters after the grid location, the CFD results deviate from the model further downstream. This is, however, not surprising, since the turbulence is not entirely homogenous isotropic (*i.e.* the production of turbulent kinetic energy still exists), and also the curve-fit is not found for the circular grids. Furthermore, the flow after the grid will start to interact with the medium surrounding the flow, and this causes further production of turbulent kinetic energy and therefore faster growth of the eddies.

4 Numerical Results and Discussions

This section is concerned with noise prediction using Lighthill's Acoustic Analogy. Before proceeding with the integrations, as given in Equation (8), one needs to find the calibrating coefficients used in the Acoustic Analogy. The length- and time-scale coefficients must be found by best fitting to data at 90 degrees (in the absence of refraction and convection effects). They are found to be $c_\tau = 1.1$, $\Upsilon^2 c_l^3 = 0.1372$, $c_s/2\pi = 3.58$.

Figure 5 compares the source distribution, $S_x(x)$, of an isolated $M = 0.75$ jet at different frequencies. The source distribution can be found by taking the overall intensity as an integral over the axial

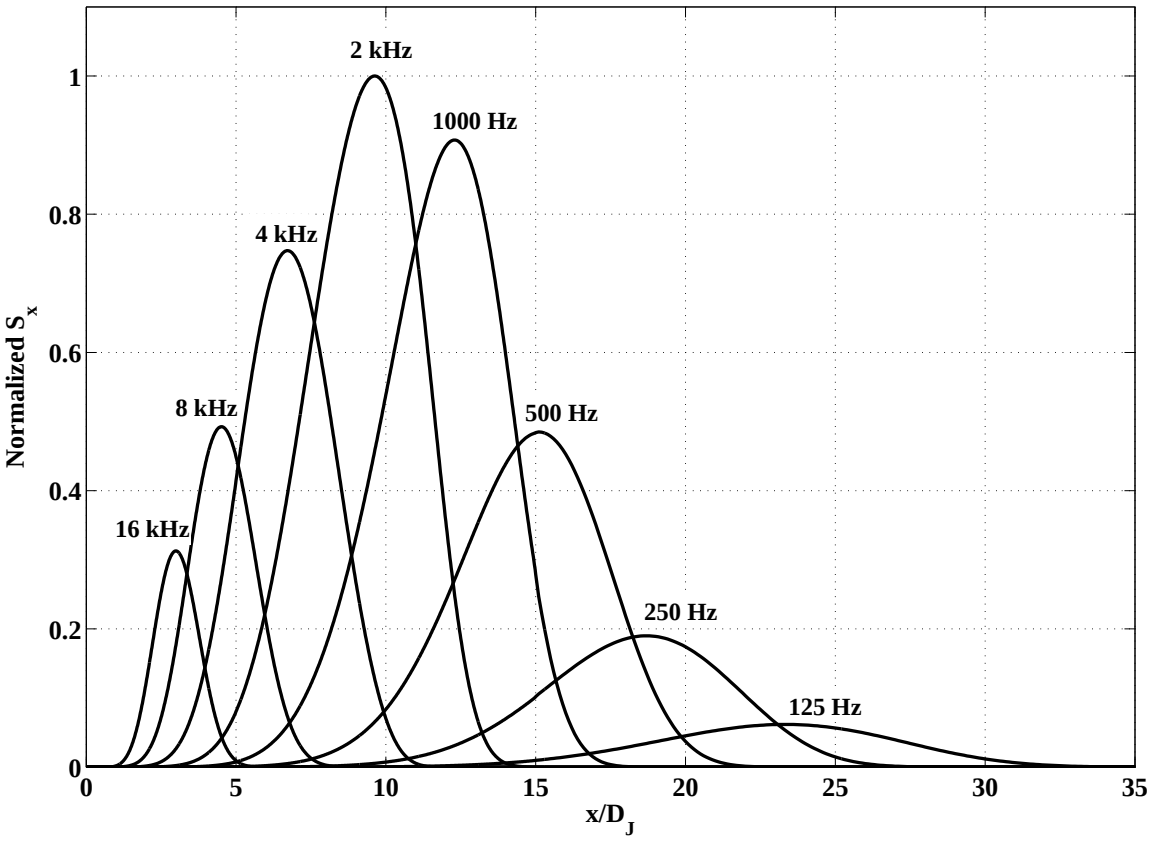

FIGURE 5: Jet noise source distribution at different frequencies; $M = 0.75$

extent of the jet, as $S(x,\omega) = \int S_x(x,\omega)dx$. Results are normalized to unity. It can be seen that the peak frequency (between $1kHz$ and $2kHz$) is formed by the sources aggregated in the region of $8 < x/D_J < 12$. While most of the sources within the first $8D_J$ only contribute to the high frequency part of the spectrum, the low frequency noise originates from the large eddies spread further downstream, $x/D_J > 12$. As mentioned earlier, in order to reduce to the low frequency noise, one needs to break down the large eddies, and also reduce their turbulent intensity. To do so, the grid should be placed somewhere before the large structures start to develop. In the jet turbulence problem, this would be near or right after the end of the potential core ($x \approx 5D_J$ to $7D_J$). Therefore, in this study, three locations are chosen $6D_J$, $8.6D_J$, and $12D_J$. In what follows, the grid with 10 rectangular cross-section rods is only used.

Figure 6 illustrates the results for the noise radiated from an isolated jet and when the grid is placed

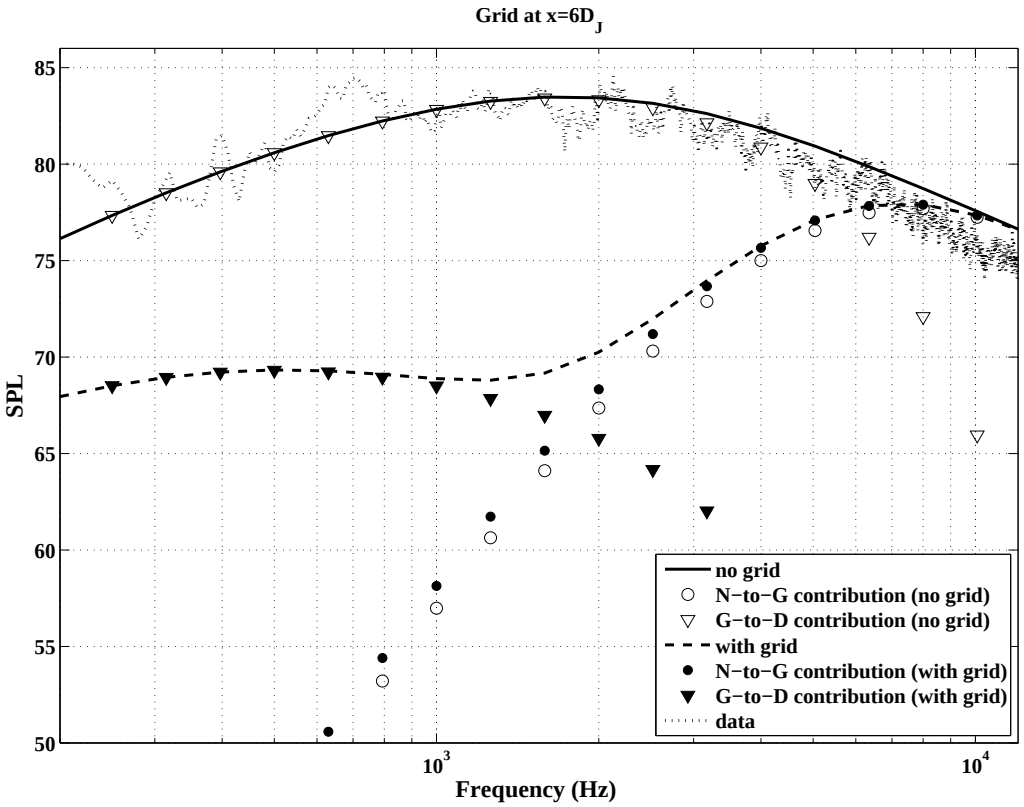

FIGURE 6: Comparison of noise from a $M = 0.75$ jet with and without a grid; grid is located at $6D_J$ downstream, $R = 50D_J$, $\theta = 90^o$.

at $6D_J$ downstream. In this figure, *"N to G"* refers to the contribution from the sources in the region between the nozzle exit to the grid location, *"G to D"* denotes the noise contribution from sources aggregated between the grid location and the jet downstream ($30D_J$). It can be easily seen that the noise contribution from the G-D region has dramatically decreased by placing the grid at $6D_J$. Results show that up to $15dB$ noise reduction can be achieved at $1000Hz$. It can also be seen that using the grid leads to slight increase in the noise level from the N-G portion, which is due to the high intensity regions produced backside of the grid as a results of flow impingement.

Figure 7 presents the results when the grid is located at $8.6D_J$ downstream. Results of the isolated jet show that the sources in the upstream region of $8.6D_J$ contribute only to the high-frequency part of the spectrum, while those aggregated in the downstream region of $8.6D_J$ form the low-frequency part of the spectrum. In other words, sources gathered around this point ($8.6D_J$) contribute the most to the

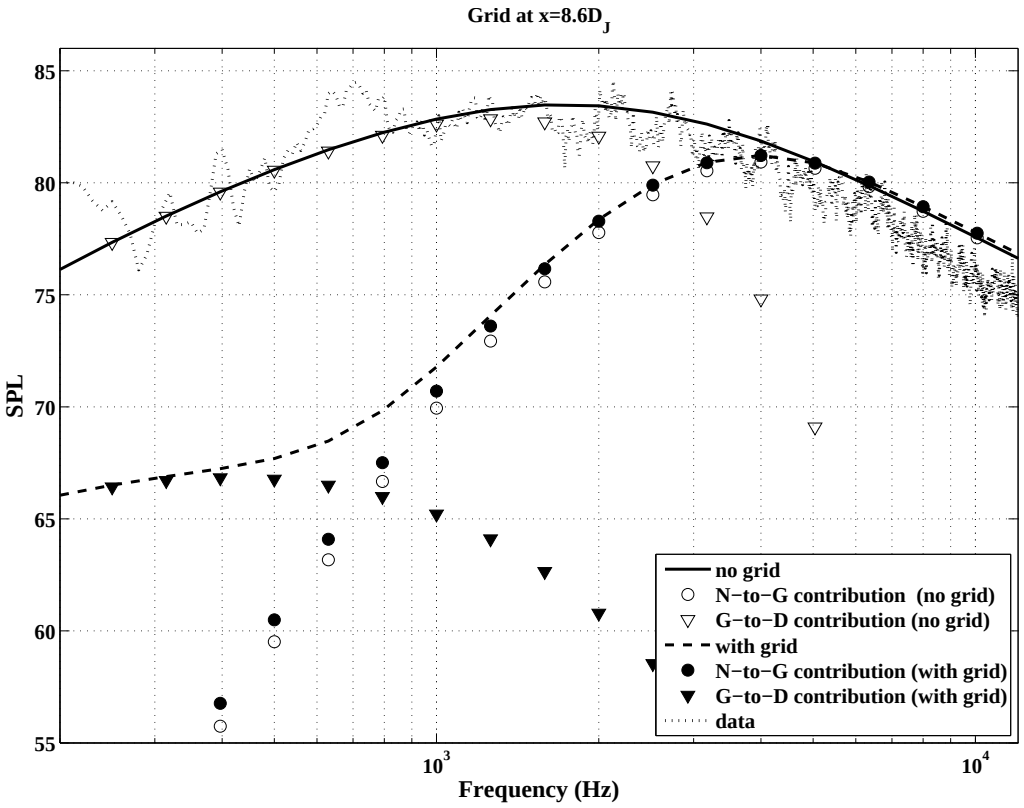

FIGURE 7: Comparison of noise from a $M = 0.75$ jet with and without a grid; grid is located at $8.6D_J$ downstream, $R = 50D_J$, $\theta = 90^o$.

peak frequency. It is therefore of great importance to study the effect of locating a grid at this point. Results have shown again that the grid can significantly reduce the noise production at low frequencies by breaking the eddies contributing to the $100-1000Hz$ band of the spectrum. Furthermore, from the comparison of figures 6 and 7 one can realize that a greater level of noise reduction can be achieved when the grid is located further downstream of the end of the potential core (about $8.6D_J$). As mentioned earlier, this is the region that is believed to be the most important contributor to the jet noise production mechanism. Moreover, a negligible increase in the high frequency part of the spectrum can also be observed which is due to impingement noise.

In the last case, we have placed the grid at $12D_J$ downstream, inside the fully developed region, see figure 8. As it can be observed from the figure, the grid is still able to reduce the radiated noise at very low frequencies, but it has not had a significant effect on the peak frequency. This implies that the

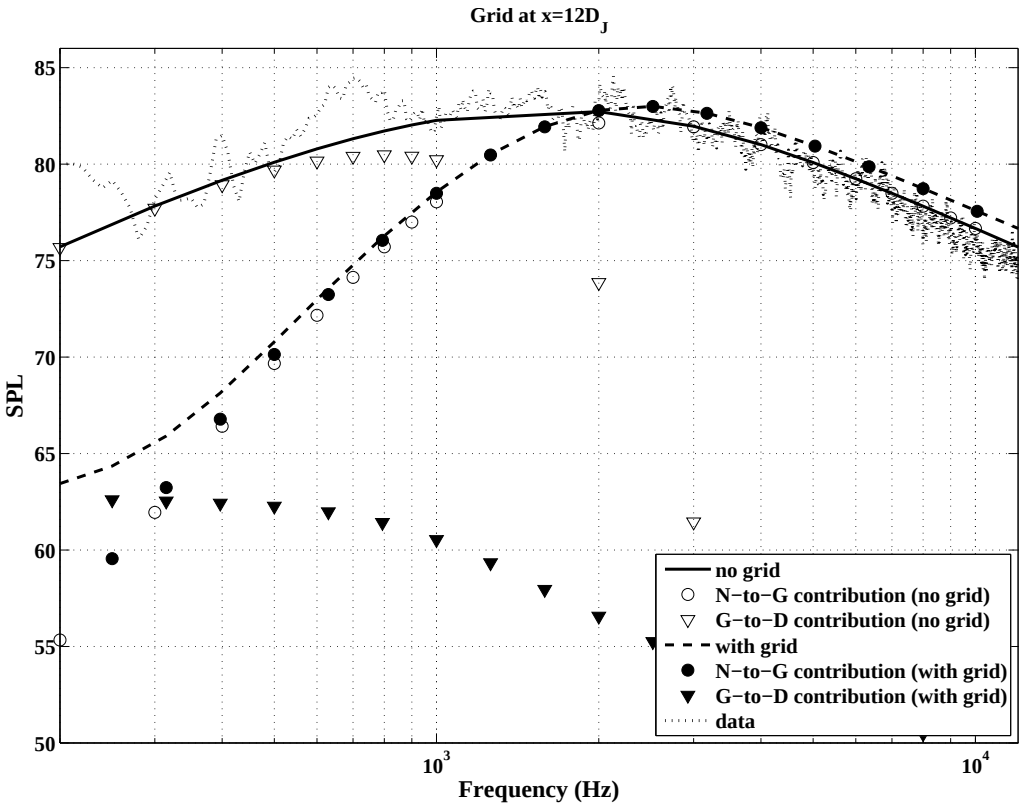

FIGURE 8: Comparison of noise from a $M = 0.75$ jet with and without a grid; grid is located at $12D_J$ downstream, $R = 50D_J$, $\theta = 90^o$.

sources responsible for forming the peak frequency are located behind the grid, as mentioned earlier.

Having studied the noise reduction using a fixed grid, a list the side effects of using such a system needs to be given as well. The most important effects are as follows: (1) Vortex sheet; flow induced vibration; and turbulent buffeting: When the vortex shedding frequency coincides with the rods natural frequency or gets close to the natural frequency, resonance takes place. For a crossflow over a single tube the Strouhal number is an almost constant value of 0.2 for Reynolds numbers up to $3.5\,10^6$ [15]. The high turbulence is also a source of structural excitation (*i.e.* turbulent buffeting). A complete review of the excitation frequency for the problem of vortex- and turbulence-induced vibration can be found in [16]. Moreover, an inclusive list of formulations for calculating rod's natural frequencies with different end conditions can be found in Refs. [17, 18]. (2) Impingement noise: The flow impinging the wires produces a high turbulence intensity region, see figure 3. However, these

regions are very small, and the noise sources aggregated there are of very high frequencies, which has not been the concern of this paper.

In the end, it is worth mentioning here some of the possible ways for further improvement of this noise reduction system:

1. Using a double or multi-layer grid instead of a single-layer screening structure can significantly improve the efficiency of the noise reduction. This will make it easier to eliminate the TKE production, which is responsible for development of new large structures.

2. Using vibrating grids results in a faster decaying turbulence. This will consequently help for greater noise reduction.

3. It is important to remind that the approach used here for the jet noise problem, can be used in a similar fashion for other kinds of aeroacoustic problems, such as cavity noise, boundary layer noise, rotating objects noise, *etc.* The only important issue here is that the turbulence structure changes from one case to another, and one needs to carefully study the turbulence characteristics of the flow before placing the grid.

5 Conclusion

This paper has considered a well recognized turbulence idea, namely grid turbulence, to be utilized for aeroacoustic purposes. A 2D circular grid has been placed inside a jet flow and the radiated noise from the new turbulence medium has been compared with that of an isolated jet flow. Results have shown that significant low frequency noise reduction can be achieved provided that the grid is placed where the large eddies begin to appear. Furthermore, in this paper provides a list of the disadvantages of this noise control system and also suggestions for greater noise reduction.

Acknowledgments

The author is grateful to members of the JEAN test programmes for the provision of experimental data used in this paper.

References

[1] Mohamed Gad el Hak, Andrew Pollard, and Jean-Paul Bonnet. *Flow Control, Fundamentals and Practices*. Springer-Verlag, Berlin Heidelberg, 1998.

[2] Mohamed Gad el Hak. *Flow Control: Passive, Active, and Reactive Flow Management*. Cambridge University Press, 2000.

[3] N. P. Mikhailova, E. U. Repik, and Yu. P. Sosedko. Scale of grid and honeycomb-generated turbulence. *Fluid Dynamics*, 36(1):69–79, 2001.

[4] S. B. Pope. *Turbulent Flows*. Cambridge University Press, Cambridge, 2003.

[5] E. J. Hopfinger and J. A. Toly. Spatially decaying turbulence and its relation to mixing across density interfaces. *J. Fluid Mech.*, 78(1):155175, 1976.

[6] Nian-Sheng Cheng and Adrian Wing-Keung Law. Measurements of turbulence generated by oscillating grid. *Journal of Hydraulic Engineering*, 127(3):201–208, 2001.

[7] P. J. Zwart, R. Budwig, and S. Tavoularis. Grid turbulence in compressible flow. *Experiments in Fluids*, 23:520–522, 1997.

[8] M. E. Goldstein. *Aeroacoustics*. McGraw-Hill, New York, 1976.

[9] A. Khavaran, J. Bridges, and J. B. Freund. A parametric study of fine-scale turbulence mixing noise. *AIAA 2002-2419*.

[10] M. Azarpyvand and R. Self. Noise prediction of a short-cowl jet using energy transfer rate time-scale. *14th AIAA/CEAS Aeroacoustics Conference, AIAA 2008-2937*.

[11] G. J. Page, J. J. McGuirk, M. Hossain, R. H. Self, and A. Bassetti. A CFD coupled acoustics approach for coaxial jet noise. *AIAA 2003-3286*.

[12] M. Harper-Bourne. Jet near field noise prediction. *AIAA/CEAS 2002-2554*.

[13] P. J. Morris and S. Boluriaan. The prediction of jet noise from CFD data. *AIAA/CEAS 2004-2977*.

[14] M. Billson. *Computational techniques for turbulence generated noise*. PhD thesis, Chalmers University of Technology, 2004.

[15] L. L. Faulkner. *Heat Exchanger Design Handbook*. Marcel Dekker, Inc., New York, 2000.

[16] T. Nakamura and S. Kaneko. *Flow Induced Vibrations: Classifications and Lessons from Practical Experiences*. Elsevier, 2008.

[17] S. Braun, D. Ewins, and S. S. Rao. *Encyclopedia of Vibration*. Academic Press, Cornwall, UK, 2001.

[18] R. D. Blevins. *Formulas for Natural Frequency and Mode Shape*. Krieger, Malabar, FL, 1984.